Immobilization of Recombinant Vault Nanoparticles on Solid Substrates

Yun Xia,[†,¶] Yamini Ramgopal,[†,¶] Hai Li,[†] Lei Shang,[§] Parisa Srinivas,[‡] Valerie A. Kickhoefer,[⊥] Leonard H. Rome,[⊥] Peter R. Preiser,[‡] Freddy Boey,[†] Hua Zhang,[†,*] and Subbu S. Venkatraman[†,*]

[†]School of Materials Science and Engineering, [‡]School of Biological Science, [§]School of Mechanical and Aerospace Engineering, Nanyang Technological University, Singapore 639798, and [⊥]Department of Biological Chemistry, and California NanoSystems Institute, University of California, Los Angeles, Los Angeles, California 90095. [¶]These authors contributed equally to this work.

ABSTRACT Native vaults are nanoscale particles found abundantly in the cytoplasm of most eukaryotic cells. They have a capsule-like structure with a thin shell surrounding a "hollow" interior compartment. Recombinant vault particles were found to self-assemble following expression of the major vault protein (MVP) in a baculovirus expression system, and these particles are virtually identical to native vaults. Such particles have been recently studied as potential delivery vehicles. In this study, we focus on immobilization of vault particles on a solid substrate, such as glass, as a first step to study their interactions with cells. To this end, we first engineered the recombinant vaults by fusing two different tags to the C-terminus of MVP, a 3 amino acid RGD peptide and a 12 amino acid RGD-strep-tag peptide. We have demonstrated two strategies for immobilizing vaults on solid substrates. The barrel-and-cap structure of vault particles was observed for the first time, by atomic force microscopy (AFM), in a dry condition. This work proved the feasibility of immobilizing vault nanoparticles on a material surface, and the possibility of using vault nanoparticles as localized and sustainable drug carriers as well as a biocompatible surface moiety.

KEYWORDS: vaults · self-assembly · RGD · strep-tag · TEM · AFM

Vaults, first described in 1986, are 13 MDa ribonucleoprotein particles, which are highly conserved in most eukaryotes.[1] There are between 10^4 and 10^6 vault particles in the cytoplasm of most eukaryotic cells. Although many different functions have been proposed for the vaults, including roles in nucleocytoplasmic transport, multidrug resistance, and innate immunity, their normal cellular function remains undetermined.[2−4] Native vaults, purified from rat liver, consist of a small untranslated RNA[5] and multiple copies of three proteins. MVP (99 kDa) makes up more than 70% of total vault mass.[6] Interestingly, the expression of MVP alone in the insect cells, which are infected with a baculovirus containing an MVP cDNA, can result in self-assembly of the MVP into the distinctive barrel-and-cap structure.[7] Thus multimerization of this protein is sufficient to form the exterior shell of the particle. The other two vault-associated proteins are vault poly-ADP-ribose polymerase (VPARP, 193 kDa) and telomerase associated protein 1 (TEP 1, 290 kDa).[8,9]

Reconstruction images, taken on the cryo-electron microscope (cryoEM), revealed the vault to be a hollow, barrel-shaped "particle" with two protruding caps and an invaginated waist.[10] Its maximum dimensions are about 42 × 42 × 75 nm^3, larger in size and mass than some icosahedral viruses. Coupled with the cryoEM analysis, a 9 Å draft crystal structure of an empty vault built from a cysteine-tagged construct of MVP indicated that each vault is composed of two identical halves; 48 copies of MVP are believed to make up each half with 6 MVPs corresponding with each "flower petal" in 8-fold symmetry.[11] All of the MVP N-termini noncovalently come together around the barrel waist in the lumen and extend toward the interior of the particle, whereas the C-termini of the MVP are collected at the barrel caps (48 on each cap).[12] Recently, Tanaka *et al*. reported the structure of rat liver vault at 3.5 Å resolution, revealing that vault cage structure consists of a dimer of half-vaults, with each half-vault comprising 39 identical MVP chains.[13] Nevertheless, for the purposes of this work, we can state that vaults have a capsule-like structure with a thin shell (*ca*. 2 nm) surrounding a large hollow interior compartment with a volume of 5 × 10^4 nm^3, which is capable of accommodating hundreds of proteins.[11] In addition, the vaultlike particles are self-assembled, natural proteins found in the normal human cells. This ensures a reasonable degree of biocompatibility for vaults. These attributes make vaults the very promising vehicles for delivery of therapeutic agents. Recombinant vault has been shown to encapsulate a semiconducting polymer, and pH lability of cross-linked vaults may

*Address correspondence to ASSubbu@ntu.edu.sg, HZhang@ntu.edu.sg.

Received for review September 6, 2009 and accepted February 4, 2010.

Published online February 10, 2010. 10.1021/nn901167s

be useful for controlled release of encapsulated materials.[14,15]

Several strategies could be used to engineer vault nanoparticles with additional properties to increase their versatility as in drug delivery system. One of them is through a vault targeting peptide found in VPARP at its C-terminus (aa 1563−1724), which is known to bind to MVP in the vault lumen.[16] This vault-targeting peptide sequence has been designated as mINT, minimal interaction domain. Fluorescent or enzymatic proteins, fused to mINT, are directed to the lumen of recombinant vaults, while retaining their native properties.[17] Difference mapping has shown that the mINT domain binds to the inside of the recombinant vaults at two locations, above and below the waist of the vault particles. Protein tags can be introduced at MVP C-terminus. It was reported that 11 amino acid epitope tag (VSVG), a 33 amino acid IgG-binding peptide, and the 55 amino acid epidermal growth factor (EGF) were fused onto the MVP C-terminus, and provided the ability to target vaults to specific cells as delivery vehicles.[18]

However, all of the previously reported work to date, which explored the possibility of vaults as a drug/protein delivery system, has used vaults in aqueous solutions. Under these conditions, generally the release of drug/peptide is not controlled or sustained to any great extent, as the vault is a dynamic, "breathing" entity. To control the release of encapsulated bioactivities, vaults may need to be incorporated into solid matrices or onto substrates, but this is difficult to accomplish, as they tend to lose their shape/structure when immobilized on a dry surface. Therefore, our aim of this study is to explore the possibility of immobilizing the vaults on a solid substrate to provide a means for localized and sustained drug release.

CP-MVP vault is the recombinant vault with each MVP having an N-terminus modified with a cysteine-rich, 12-amino acid peptide tag derived from the metallothionine protein. They are found to be the most stable vault constructs thus far produced with consistent size, shape and conformation.[11,12] RGD (Arg-Gly-Asp) peptide is a well-known cell affinity ligand found in extracellular matrix, which binds to the cell membrane protein, integrin. In this study, we added the 3 amino acid RGD peptide onto the C-terminus of CP-MVP to form CP-MVP-RGD. We also produced CP-MVP-RGD-STP by fusing an additional (9 amino acid) strep-tag to the C-terminus of CP-MVP-RGD. We report two methods to immobilize vault particles on glass, through covalent bonding and electrostatic adsorption. For the first time, we have observed the vault particles on glass by AFM in the "dry" state after immobilization.

RESULTS AND DISCUSSION

Structural Characterization of C-Terminally Tagged Vaults. The C-terminus of MVP is localized in the "caps of the barrel",[12,13] and peptide additions are accessible.[18] In this study, in addition to CP-MVP, two types of C-terminally tagged recombinant vault particles, CP-MVP-RGD and CP-MVP-RGD-STP, were expressed by Bac-to-Bac Baculovirus expression system as described previously.[7] The expression of RGD at the C-termini of vault particles would be expected to lead to an increase of cell adhesion on the vault-immobilized substrate. Strep-tag is wildly used in protein purification and detection because of its strong affinity to streptavidin. The expression of the additional strep-tag at the C-terminus of CP-MVP-RGD is solely for detection of C-terminal tag expression, that is, confirming the incorporation of RGD sequence in MVP. The successful expression of strep-tag at C-terminus of MVP has an additional advantage, as explained below.

Fractionation on a discontinuous sucrose gradient is the most important step during vault purification. Generally, vaults fractionate in the 40% and 45% layer depending on whether or not the particles are empty or filled with mINT fusion proteins (in this study, we used the mCherry-mINT protein for confirming the self-assembled structure, as explained below). Empty particles are found in higher concentrations in the 40% layer, and filled particles fractionate in the 45% layer. Recombinant CP-MVP (Figure 1A, lane 1) as positive control, CP-MVP-RGD (Figure 1A, lane 2) and CP-MVP-RGD-STP (Figure 1A, lane 4), purified from the 40% sucrose gradient fractions, were analyzed by immunoblotting with anti-MVP antibody. All three fractions contained MVP, indicating that proper vaults were formed for the three different constructs. S20 extract of Sf9 cells without infection of any baculovirus was analyzed as negative control (Figure 1A, lane 3), and showed no MVP production. To establish whether the C-terminal tags were functionally exposed, a pull-down experiment with streptavidin beads was carried out. S20 extracts of CP-MVP-RGD-STP and CP-MVP-RGD were used for binding experiments, followed by subsequent immunoblotting analysis with anti-MVP antibody. S20 extracts of CP-MVP-RGD-STP and CP-MVP-RGD contained MVP as detected by Western blot (Figure 1B, lanes 1 and 3) with only CP-MVP-RGD-STP being successfully purified by streptavidin beads, compared to CP-MVP-RGD (compare Figure 1B, lanes 2 and 4). This confirms that the RGD-STP and by analogy the RGD tag on its own were successfully cloned in frame with the MVP, and that the RGD tag was functionally exposed to the outside of the vault particles. Importantly, the use of streptavidin beads to purify vaults from S20 extracts may in future be a valuable technique for large-scale purification of vaults, which is very difficult to achieve using the current sucrose gradient approach.

In this study, a fluorochrome (mCherry) was also incorporated into the vault by attaching to the previously defined vault-targeting domain, mINT. Purified recombinant vaults (CP-MVP-RGD/mCherry-mINT and CP-

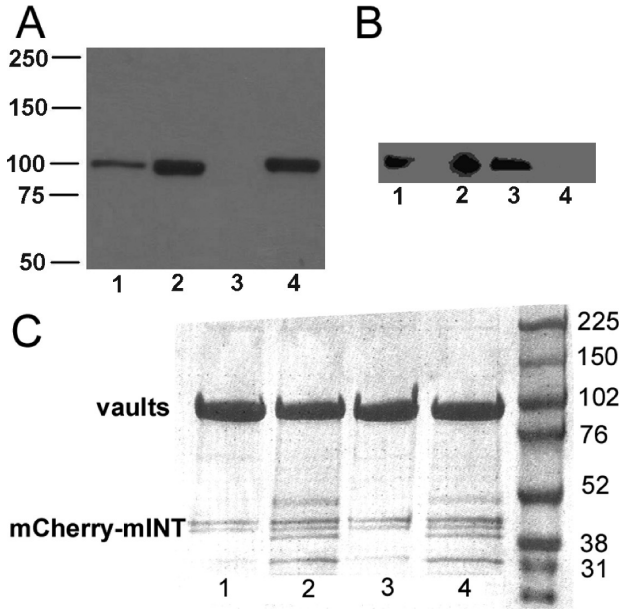

Figure 1. The C-terminal peptide tag is located on the exterior of the caps of recombinant vaults. (A) Western blot analysis of purified CP-MVP-RGD (lane 2) and CP-MVP-RGD-STP (lane 4), compared with CP-MVP as positive control (lane 1), and S20 extract Sf9 cells without any baculovirus infection as negative control (lane 3). (B) Western blot analysis of streptavidin beads affinity purified proteins from S20 extracts. Lane 1 and lane 3 are from S20 extracts of CP-MVP-RGD-STP and CP-MVP-RGD, respectively. Lane 2 and lane 4 are from bead affinity test of CP-MVP-RGD-STP and CP-MVP-RGD, respectively. (C) Coomassie stain of purified CP-MVP-RGD-STP (lane 1, 40% fraction and lane 2, 45% fraction) and CP-MVP-RGD (lane 3, 40% fraction and lane 4, 45% fraction) recombinant vaults containing mCherry-mINT fractionated on 4−15% SDS-PAGE. The major protein bands are the ~100 kDa CP-MVP-RGD/CP-MVP-RGD-STP and the ~45 kDa mCherry-mINT (note: the 45 kDa mCherry-mINT is a triplet that is likely caused by leaky translation due to the presence of three in-frame methionines in the first 17 amino acids of mCherry).[18]

MVP-RGD-STP/mCherry-mINT) were studied by coomassie staining (Figure 1C), showing that mCherry-mINT was successfully copurified with the vaults and was enriched in the 45% sucrose gradient layer. This strongly suggests that both the CP-MVP-RGD and the CP-MVP-RGD-STP constructs produce the fully assembled vaults.

For the final confirmation of the correct assembly of the vault with the C-terminal tagged MVP, the morphology of assembled CP-MVP, CP-MVP-RGD, and CP-MVP-RGD-STP vault particles was further analyzed by transmission electron microscopy (TEM), demonstrating the abundant, barrel-shaped recombinant particles (Figure 2). These particles varied from 32−37 nm in width and 59−65 nm in length, and displayed the distinctive bifold symmetric central barrel of the vault with dual caps.

Vault Particles Immobilization on APTES-Modified Glass Substrate. Our aim is to demonstrate the feasibility of immobilizing vault particles on a substrate for studies of cellular interaction and/or localized drug/gene delivery. Glass was selected as the substrate, as it is easily functionalized with silanes. Two strategies were developed. The first method is based on the electrostatic adsorption. Vault particles are reported to be negatively charged overall. We found that the vault particles could be easily adsorbed on a positively charged APTES-modified glass surface. The second method is based on the covalent bonding between the amine groups in the APTES-modified surface and the carboxylic groups in the exposed C-termini of vault particles in water-soluble carbodiimide (WSC) solution (Scheme 1). There are between 39 and 48 C-termini localized at each vault half at the caps, and exposed outside of the vault particle.

As mentioned above, CP-MVP and CP-MVP-RGD vault particles used in this study contain the fluorescent proteins, mCherry-mINT. The mINT domain on mCherry-mINT is able to interact with MVP, and to direct mCherry-mINT into the lumen of the recombinant vaults. Nonspecific bound vaults with mCherry-mINT can be washed away; hence any detected fluorescence indicates the presence of half-assembled or fully assembled vaults. It means that the amount of structurally assembled vaults immobilized on substrate can be quantified by measuring the mCherry fluorescent intensity. As mINT domain binds the inside of vaults at at two locations, above and the below the waist of the vault particles, detection of mCherry fluorescent intensity confirms the presence of

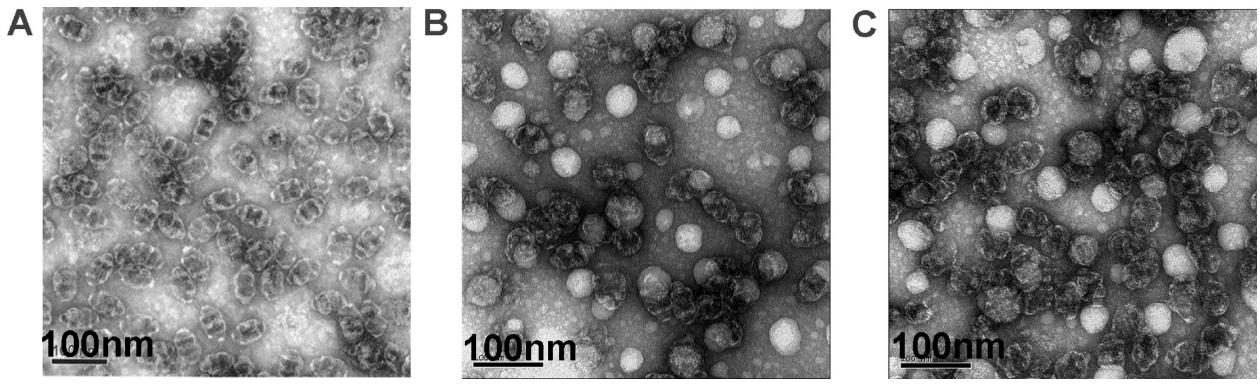

Figure 2. TEM micrograph of the negative-stained recombinant (A) CP-MVP, (B) CP-MVP-RGD, and (C) CP-MVP-RGD-STP vault particles.

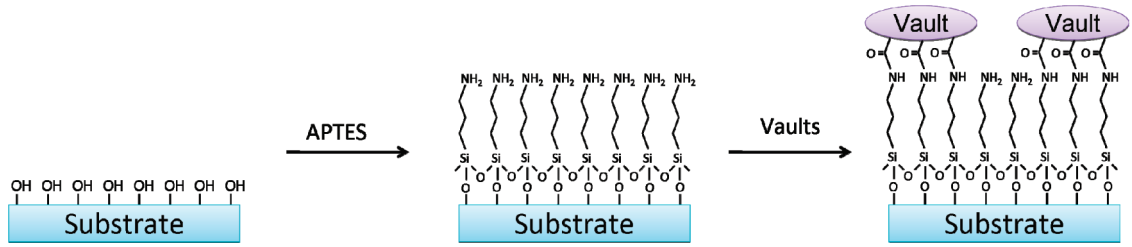

Scheme 1. Immobilization of vault particles on an APTES-modified glass substrate in a carbodiimide solution based on the covalent bonding.

full- or half-assembled vaults, and cannot unequivocally confirm the fully assembled structure.

The protein concentration of purified vaults containing mCherry-mINT (CP-MVP/mCherry-mINT) was measured using the standard bicinchoninic acid assay (BCA). The fluorescent intensity of CP-MVP/mCherry-mINT solution corresponding to different total protein concentrations was measured by fluorescent microplate reader. Thus, the vaults quantification calibration curve could be established by plotting mCherry fluorescent intensity against vault concentration (Figure 3). The above calibration was used to quantify the amount of half- and fully-assembled vaults on the substrates by measuring the fluorescence intensity, and the results are tabulated below (Table 1).

In general, the mCherry-mINT data showed that the vaults can be immobilized on APTES-modified glass surface, and further that a substantial portion of the original vault loading is immobilized in the half-vault or full-vault configuration. Both types of vaults, CP-MVP and CP-MVP-RGD, could be immobilized by electrostatic adsorption or covalent bonding, although the relative efficiency was somewhat different. The preference for either method will depend on the nature of the application, which could be influenced by the stability of the immobilized vaults.

Surface Characterization of Vaults-Immobilized Glass Substrates. The mCherry-mINT fluorescent intensity measurement was carried out in an aqueous environment

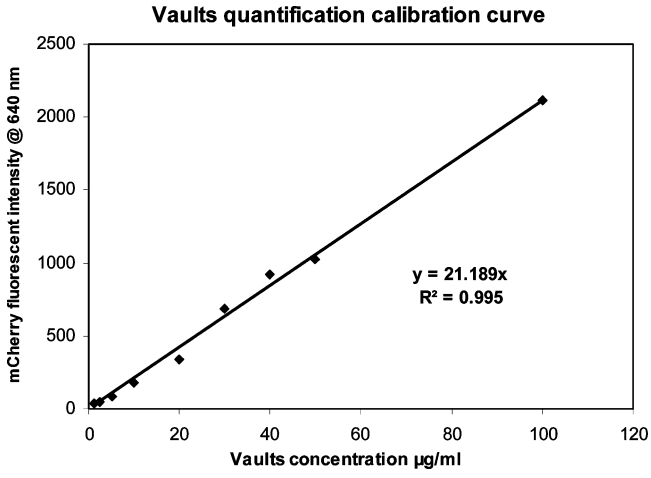

Figure 3. The calibration curve for vaults, with a fluoroscent "tag" CP-MVP/mCherry-mINT. The fluoroscent intensity was measured at excitation wavelegth of 540 nm and emission wavelength of 640 nm.

for the vaults, and it would be instructive to check whether this configuration is maintained in a "dry" environment, as it will be critical for some applications. We report on efforts to do this in this section.

First, we characterized the surface (in a dry state) for the presence of vaults as well as the success of the surface functionalization. To do this, after the substrate was coated with vault particles, it was dried in vacuum oven at 37 °C for 12 h. The chemical and structural stability of the immobilized vaults was studied by various surface characterization techniques. To confirm the success of silanization on glass, and to characterize surface chemical composition of the vaults-coated substrate, X-ray photoelectron spectroscopy (XPS) was carried out on bare glass, APTES-modified glass, CP-MVP-coated APTES-modified glass, and CP-MVP-RGD-coated APTES-modified glass (Figure 4). The atomic percentage was tabulated in Table 2, together with the measured nitrogen to carbon ratio (N/C ratio), compared with the theoretical N/C ratio. On a bare glass, no nitrogen peak was detected. The presence of the N1s peak at *ca.* 400 eV on the APTES- modified glass was a strong evidence of existence of the APTES layer. The N/C ratio of APTES-modified glass was expected to be from 0.14 to 0.33 depending on the degree of hydrolysis of ethoxy groups into silanol groups.[19] The measured N/C ratio of 0.16 was reasonably within its theoretical range. CP-MVP and CP-MVP-RGD-coated APTES-modified glass showed N1s peaks as well. As MVP is a large protein with molecular weight around 100 kDa, its theoretical N/C ratio was calculated by taking the average N/C ratio of the most common 20 amino acids. The N/C ratios measured on vaults-coated substrates were about 0.21−0.23, which were slightly higher than that measured on APTES- modified glass. However, this N1s peak might arise from vaults as well as from the exposed APTES layer on glass. The protein nature of CP-MVP and CP-MVP-RGD coating on APTES-

TABLE 1. The Loading Efficiency of Vault Immobilization on APTES-Modified Glass

	covalent bonding		electrostatic adsorption	
	CP-MVP	CP-MVP-RGD	CP-MVP	CP-MVP-RGD
immobilized amount (μg)	1.98	1.79	2.13	1.32
loading amount (μg)	4	4	4	4
loading efficiency	49.5%	44.8%	53.2%	33.1%

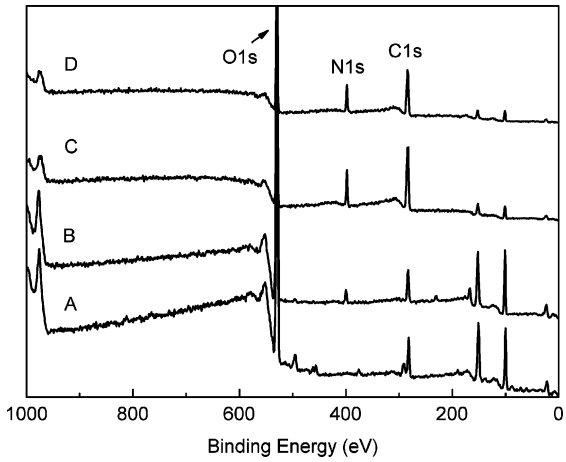

Figure 4. XPS spectra of (A) bare glass, (B) ATPES- modified glass, (C) CP-MVP-coated APTES-modified glass, and (D) CP-MVP-RGD-coated APTES-modified glass.

modified glass was therefore further characterized by attenuated total reflection Fourier transform infrared spectroscopy (ATR-FTIR).

The ATR-FTIR measurement of the vault layer was performed using a bare glass as the background. In Figure 5A, APTES-modified glass, coated with CP-MVP based on electrostatic adsorption, showed the characteristic peaks of amide I bond around 1650 cm^{-1}, which was assigned to the carboxyl stretching.[20] A similar spectrum was observed on APTES-modified glass, coated with CP-MVP-RGD. Both main chains of immobilized vaults and APTES-vault covalent coupling are able to contribute to amide I signal. However, main chains of immobilized vaults on substrate should be the main signal source. That means the observation of amide I peak only proved the presence of proteins on the substrate, that is, the immobilized recombinant vault proteins. The self-assembled vault structure has to be confirmed by other topological techniques, such as AFM. The characteristic N−H stretching peak around 3200−3400 cm^{-1} from APTES was also observed, arising from the incomplete surface coverage of vaults on APTES-modified glass.[21]

TABLE 2. Atomic Percentage and N/C Ratio of (A) Bare Glass, (B) ATPES-Modified Glass, (C) CP-MVP-Coated ATPES-Modified Glass, and (D) CP-MVP-RGD-Coated ATPES-Modified Glass

			atomic percentage %		
sample	measured N/C ratio	theoretical N/C ratio	O 1s (532 eV)	N 1s (400 eV)	C 1s (285 eV)
A	0	0	75.69		24.31
B	0.16	0.14−0.33[a]	72.15	3.83	24.02
C	0.21	0.33	26.81	12.61	60.58
D	0.23	0.33	27.81	13.56	58.63

[a]Because of incomplete hydrolysis of ethoxy groups, theoretical N/C ratio of APTES-modified surface ranges from 0.14, with hydrolysis of one ethoxy group, to 0.33 with hydrolysis of three ethoxy groups.[19]

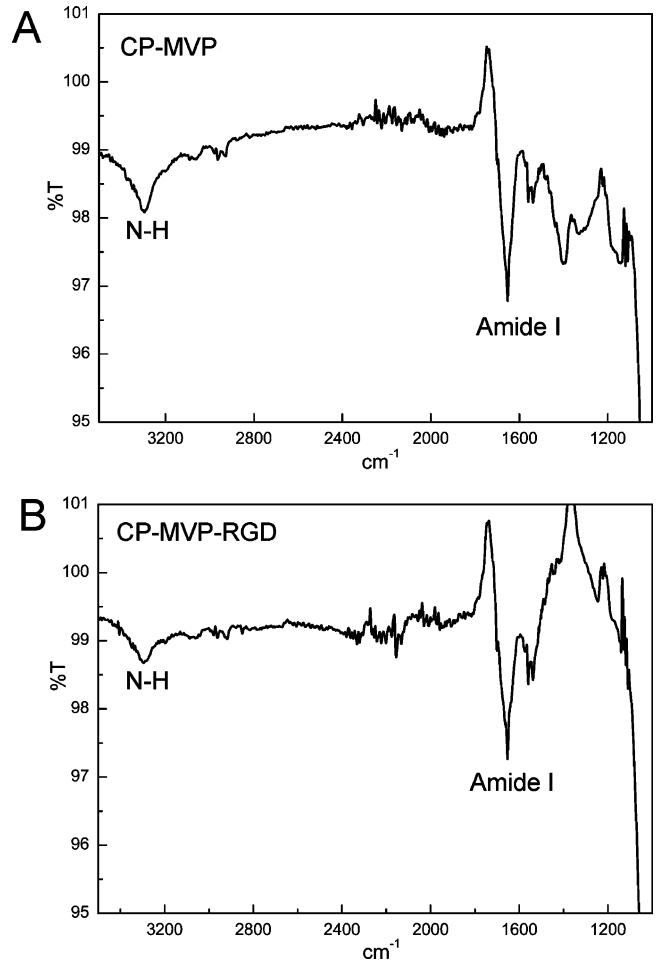

Figure 5. ATR-FTIR spectra of (A) CP-MVP immobilized on APTES-modified glass and (B) CP-MVP-RGD immobilized on APTES-modified glass. The amide I bond is assigned to C═O stretching shown in 1600−1690 cm^{-1}.

XPS and ATR-FTIR techniques yield no information about whether the recombinant vaults assumed the characteristic barrel-and-cap structure after they were immobilized on the surface. It is not possible to image the vaults on a glass substrate by TEM, therefore the CP-MVP and CP-MVP-RGD vault particles-coated, APTES-modified glass coverslips were imaged by AFM (these glass coverslips were dried after the coatings were applied, hence are in a nonaqueous environment). It was found that the vaults adsorbed on the substrate (Figure 6A−E), and their characteristic barrel-and-cap structure was retained. Some of the smaller particles appeared in AFM imaging as well. This might be due to the adsorbed salts coming from the solution and other contaminations, as well as due to some disassembled vaults.

In Figure 6F, TEM images of CP-MVP vault particles are compared to the AFM images. Most vault particles in AFM images are barrel-shaped and similar to those observed in TEM images. Caps at the two ends of vault particles can also be seen quite clearly. The dimensions of vault particles in AFM images are compared with those in TEM images as well. From the AFM images,

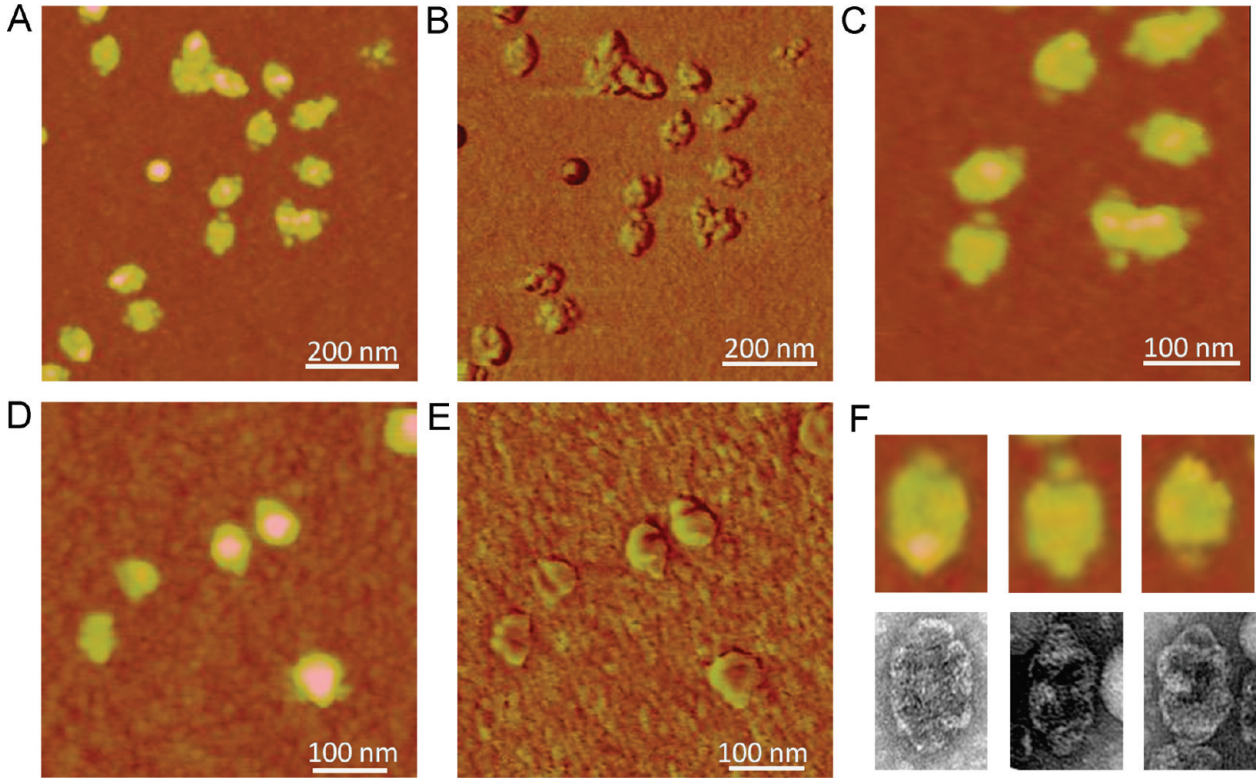

Figure 6. AFM topographic images of (A, C) CP-MVP and (D) CP-MVP-RGD adsorbed on APTES-modified glass, respectively. AFM phase images of (B) CP-MVP and (E) CP-MVP-RGD adsorbed on APTES-modified glass, respectively. (F) Comparison between AFM topographic images (top row) and TEM images (bottom row). The Z scale for AFM topographic images in panels A, C, and D is 20 nm. The Z scale for AFM phase image in panels B and E is 20° and 60°, respectively.

the observed width and length of CP-MVP vault particles are 63.2 ± 2.8 and 90.2 ± 2.1 nm, respectively. Due to the tip−sample convolution,[22] the lateral dimensions of vault particles in AFM images are larger than those in TEM images (32−37 nm in width and 59−65 nm in length). The height of CP-MVP vault particles measured by AFM is about 8 nm, which is lower than 41 nm measured by cryoEM.[11] Two possible reasons are given for this smaller vertical dimension of vaults imaged by AFM. First, at ambient conditions, the AFM tip exerts a relatively large force on the soft vault particles, sufficient to compress the vaults somewhat.[23] It was also reported that the measured height of dsDNA by tapping mode AFM in air was about 0.7 nm, though the diameter of dsDNA of 2 nm was well accepted and proven by many experiments.[24] Second, the smaller height could also be caused by the interaction between the vaults and APTES-modified glass.[25,26] Importantly, this is the first time that the barrel-and-cap structure of recombinant vault particles has been observed in a dry condition. The successful immobilization of intact vault nanoparticles on a solid substrate may open up future applications for selective cellular interactions as well as for localized delivery of bioactive agents.

CONCLUSION

We have described the production of two successful C-terminal modifications of recombinant vaults, CP-MVP-RGD and CP-MVP-RGD-STP. These RGD sequences are attached to the C-termini on the "caps" of assembled vault structures, and therefore may be utilized to advantage for cellular interactions. Two methods, that is, electrostatic adsorption and covalent bonding, were used to attach vaults to APTES-modified glass substrates. Both types of vaults (vaults with and without the RGD sequence) were attached successfully by either method to APTES-modified glass substrates. We have shown further that such immobilized vaults retain their barrel-and-cap structure even when the substrate is dried. This was observed for the first time by AFM. This work demonstrates the feasibility of immobilizing vault nanoparticles on a material surface and will be explored further for the specific applications.

MATERIALS AND METHODS

Chemicals. (3-Aminopropyl)triethoxysilane (APTES) (99%, Aldrich), 1-ethyl-3-(3-dimethylamiopropyl) carbodiimide hydrochloride (EDAC, Pierce), and 2-morpholinoethanesulfonic acid (MES, Sigma), *N*-hydroxysuccinimide (NHS), 1% Triton X-100, 1 mM dithiothreitol, 0.5 mM phenylmethylsulfonyl fluoride (PMSF), pro-

tease inhibitor cocktail, Tris HCl, glycerol, sodium dodecyl sulfate (SDS), and β mercaptoethanol bought from Sigma were used as received. All solvents were either HPLC grades or analytical grades and were purchased from Sigma and Aldrich.

Construction of Modified Recombinant Plasmids. The 3 amino acid sequence of the RGD tag is Arg-Gly-Asp. The RGD peptide is cloned in to the C-terminus or 3′ end of the rat MVP cDNA using a unique internal *XhoI* site in the 3′ end of the rat MVP cDNA (GenBank accession no. U09870). Two primers were designed. The forward primer is 5′-CAGCCCGGATCATTCGAATGGCTGTTTTTGGC-3′, which is about 80 bases upstream (5′) of the *XhoI* site in the rat MVP cDNA. The reverse primer is 5′-GCGCGGTACCTCAGTCTCCCCGCTTCTGTGCTGGCGGCTG-3′, which is complementary to the 3′ end of MVP cDNA and encodes RGD. The 3′ end of MVP was PCR amplified using forward and reverse primers with the CP-MVP pFastBac plasmid as the template. The PCR product (containing the 3′ end of the MVP cDNA fused in frame to the RGD DNA) was purified on a Qiagen column, digested with XhoI and *Kpn*I, and ligated to XhoI/*Kpn*I digested CP-MVP pFastBac DNA to form CP-MVP-RGD pFastBac. All constructs were confirmed by DNA sequence analysis.

Likewise, CP-MVP-RGD-STP is made by fusing 3 amino acid RGD peptide and 9 amino acid strep-tag to C-terminus of CP-MVP. The 12 amino acid sequence of RGD-STP tag is Arg-Gly-Asp-Ala-Trp-Arg-His-Pro-Glu-Phe-Gly-Gly. The forward Primer was designed as: 5′-CAGCCCGGATCATTCGAATGGCTGTTTTTGGCTTTGAGATGTCTGAAGACACAGGTCCTGATGGCACA-3′. The reverse was 5′-GCGCGGTACCTCAGCCGCCAAATTCCGGATGTCTCCAGGCGTCTCCCCCGCTTCTGTGCTGGCGGCTG-3′, which is complementary to the last 20 bases of the rat MVP cDNA, and encodes RGD-STP. The 3′ end of MVP was PCR amplified using RGD-STP forward and reverse primers with the CP-MVP pFastBac plasmid as the template. The PCR product (containing the 3′ end of the MVP cDNA fused in frame to the RGD-STP DNA) was purified on a Qiagen column, digested with XhoI and *Kpn*I, and ligated to XhoI/*Kpn*I digested CP-MVP pFastBac DNA to form CP-MVP-RGD-STP pFastBac. All constructs were confirmed by DNA sequence analysis.

The vault targeting construct, mCherry-mINT pFastBac, was described previously.[18]

Expression and Purification of Recombinant Vaults. Recombinant baculoviruses were generated according to the Bac-to-Bac protocol (Invitrogen). For vault purification, baculovirus-infected Sf9 insect cells were subjected to a standard protocol described previously.[7] The protein concentration of purified vault proteins was determined by using the BCA assay (Pierce), and their purity was analyzed by fractionating on SDS-PAGE gel followed by staining with Coomassie blue. All vault samples were routinely analyzed by staining with uranyl acetate and viewed on an electron microscope as previously described.[1]

Western Blot Analysis. Western blot analyses were performed as described previously,[18] using anti-MVP rabbit polyclonal antibodies as primary antibody and peroxidase-conjugated goat antirabbit IgG (BioRad) as secondary antibody.

Bead Binding Assays. Lysates of sf9 cells infected with the appropriate baculovirus were prepared by lysing cells in 50 mM Tris-Cl, pH7.4, 75 mM NaCl, 0.5 mM $MgCl_2$ containing 1% Triton X-100, protease inhibitor cocktail (Sigma), and 1 mM PMSF, followed by centrifugation at 20000*g* for 10 min. The supernatants (S20) were used for the binding assays. Streptavidin beads (Streptavidin UltraLink Resin, Pierce) were equilibrated in lysis buffer. S20 lysates from CP-MVP-RGD and CP-MVP-RGD-STP infected cells were mixed with beads for 1 h at 4 °C. The beads were then washed with phosphate buffered saline (PBS) and boiled in SDS-PAGE samples buffer. The eluted proteins were loaded onto to 6% SDS-polyacrylamide gel, transferred to a nitrocellulose membrane, and probed with polyclonal anti-MVP antibodies followed by peroxidase-conjugated goat antirabbit IgG.

Preparation of APTES-Modified Glass. Microscope glass coverslips (DI = 15 mm) were used. Prior to APTES treatment, glass coverslips were sonicated in a mixture of acetone and water (v/v = 1:1) for 15 min, and then immersed in piranha solution (H_2SO_4:H_2O_2 = 7:3 v/v) for 60 min at 120 °C. They were rinsed with copious amount of Milli-Q water and dried under a stream of nitrogen. The glass treated in this way is rich in hydroxyls at the oxide surface and suitable for silanization.[27] The cleaned glass was immersed in 1 vol % APTES in Milli-Q water for 15 min. Then the substrate was rinsed with water to remove any excess of silanes, and subsequently dried under a stream of nitrogen. APTES-modified glass was heated in oven at 120 °C for 1 h.

Immobilization of Vault Particles. (1) Immobilization with electrostatic adsorption: 4 μg vaults, dissolved in 50 μL Milli-Q water, was deposited on APTES-modified glass and kept for overnight in humid box. (2) Immobilization by covalent bonding: EDAC and NHS were added into 25 mM MES solution, pH 6.5, to form the water-soluble carbodiimide (WSC). APTES-modified glass was immersed into this WSC solution with 4 μg of protein (MVP vaults or MVP-RGD vaults) loading. The reaction was kept for 10 h at room temperature.

Quantification of Immobilized Vaults on APTES-Modified Glass Coverslips. After the immobilization reaction, glass substrates were washed with Milli-Q water to remove loosely adsorbed vault particles or free mCherry-mINT released from the broken vault particles. The amount of vault particles immobilized on APTES-modified glass was measured by fluorescent microplate reader (Tecan infinite M200) at excitation wavelength of 540 nm and emission wavelength of 640 nm. The amount of vaults immobilized on the APTES-modified glass coverslips were quantified using a standard curve constructed with mCherry fluorescent intensity against vaults particle mass.

ATR-FTIR. IR spectra were measured using a Perkin-Elmer Spectrum GX system equipped with a Graseby Specac ATR detector. For one spectrum, 256 scans were coadded at a resolution of 4 cm^{-1}. The bare glass was measured for background spectra.

XPS. The surface composition of protein-coated APTES-modified glass was analyzed by XPS (Kratos AXIS Ultra) with monochromatic Al Kα (1486.71 eV) X-ray radiation (15 kV and 10 mA); 160 eV pass energy was used for survey scan, whereas 40 eV was used for the high-resolution scan.

AFM. The protein-coated APTES-modified glass was washed by Milli-Q water and dried with nitrogen gas. A commercial AFM instrument (Dimension 3100 with Nanoscope IIIa controller, Veeco Instruments Inc., CA) equipped with a scanner (90 μm × 90 μm) was employed. The tapping mode in air was performed to observe the vault particles on APTES-modified glass. Super sharp silicon cantilevers with the normal resonance frequency of 330 kHz and spring constants of 42 N m^{-1} (SSS-NCH, Nanosensors) were used. All images were captured with scan rate at 1−2 Hz and 512 × 512 pixel resolution.

Acknowledgment. We would like to thank Nanyang Technological University for partial funding of the early stages of this work. We would also like to thank the National Research Foundation of Singapore for a Competitive Research Grant (NRF-CRP2-2007-01) that funded the later stages of this effort, and the Centre for Biomimetic Sensor Science at NTU in Singapore.

REFERENCES AND NOTES

1. Kedersha, N. L.; Rome, L. H. Isolation and Characterization of a Novel Ribonucleoprotein Particle: Large Structures Contain a Single Species of Small RNA. *J. Cell Biol.* **1986**, *103*, 699–709.
2. Chugani, D. C.; Rome, L. H.; Kedersha, N. L. Evidence that Vault Ribonucleoprotein Particles Localize to the Nuclear Pore Complex. *J. Cell Sci.* **1993**, *106*, 23–29.
3. Scheffer, G. L.; Wijngaard, P. L. J.; Flens, M. J.; Izquierdo, M. A.; Slovak, M.; Meijer, C.; Clevers, H. C.; Scheper, R. J. The Drug Resistance-Related Protein LRP Is the Human Major Vault Protein. *Nat. Med.* **1995**, *1*, 578–582.
4. Kowalski, M. P.; Dubouix-Bourandy, A.; Bajmoczi, M.; Golan, D. E.; Zaidi, T.; Coutinho-Sledge, Y. S.; Gygi, M. P.; Gygi, S. P.; Wiemer, E. A. C.; Pier, G. B. Host Resistance to Lung Infection Mediated by Major Vault Protein in Epithelial Cells. *Science* **2007**, *317*, 130–132.
5. Kickhoefer, V. A.; Searles, R. P.; Kedersha, N. L.; Garber, M. E.; Johnson, D. L.; Rome, L. H. Vault Ribonucleoprotein Particles from Rat and Bullfrog Contain a Related Small RNA That Is Transcribed by RNA Polymerase III. *J. Biol. Chem.* **1993**, *268*, 7868–7873.

6. Kedersha, N. L.; Heuser, J. E.; Chugani, D. C.; Rome, L. H. Vaults. III. Vault Ribonucleoprotein Particles Open into Flower-like Structures with Octagonal Symmetry. *J. Cell Biol.* **1991**, *112*, 225–235.
7. Stephen, A. G.; Raval-Fernandes, S.; Huynh, T.; Torres, M.; Kickhoefer, V. A.; Rome, L. H. Assembly of Vault-like Particles in Insect Cells Expressing Only the Major Vault Protein. *J. Biol. Chem.* **2001**, *276*, 23217–23220.
8. Kickhoefer, V. A.; Siva, A. C.; Kedersha, N. L.; Inman, E. M.; Ruland, C.; Streuli, M.; Rome, L. H. The 193-kD Vault Protein, VPARP, Is a Novel Poly(ADP-ribose) Polymerase. *J. Cell Biol.* **1999**, *146*, 917–928.
9. Kickhoefer, V. A.; Stephen, A. G.; Harrington, L.; Robinson, M. O.; Rome, L. H. Vaults and Telomerase Share a Common Subunit, TEP1. *J. Biol. Chem.* **1999**, *274*, 32712–32717.
10. Kong, L. B.; Siva, A. C.; Rome, L. H.; Stewart, P. L. Structure of the Vault, a Ubiquitous Celular Component. *Structure* **1999**, *7*, 371–379.
11. Mikyas, Y.; Makabi, M.; Raval-Fernandes, S.; Harrington, L.; Kickhoefer, V. A.; Rome, L. H.; Stewart, P. L. Cryoelectron Microscopy Imaging of Recombinant and Tissue Derived Vaults: Localization of the MVP N Termini and VPARP. *J. Mol. Biol.* **2004**, *344*, 91–105.
12. Anderson, D. H.; Kickhoefer, V. A.; Sievers, S. A.; Rome, L. H.; Eisenberg, D. Draft Crystal Structure of the Vault Shell at 9-Å Resolution. *PLoS Biol.* **2007**, *5*, 2661–2670.
13. Tanaka, H.; Kato, K.; Yamashita, E.; Sumizawa, T.; Zhou, Y.; Yao, M.; Iwasaki, K.; Yoshimura, M.; Tsukihara, T. The Structure of Rat Liver Vault at 3.5 Angstrom Resolution. *Science* **2009**, *323*, 384–388.
14. Ng, B. C.; Yu, M.; Gopal, A.; Rome, L. H.; Monbouquette, H. G.; Tolbert, S. H. Encapsulation of Semiconducting Polymers in Vault Protein Cages. *Nano Lett.* **2008**, *8*, 3503–3509.
15. Yu, M.; Ng, B. C.; Rome, L. H.; Tolbert, S. H.; Monbouquette, H. G. Reversible pH Lability of Cross-Linked Vault Nanocapsules. *Nano Lett.* **2008**, *8*, 3510–3515.
16. van Zon, A.; Mossink, M. H.; Schoester, M.; Scheffer, G. L.; Scheper, R. J.; Sonneveld, P.; Wiemer, E. A. C. Structural Domains of Vault Proteins: A Role for the Coiled Coil Domain in Vault Assembly. *Biochem. Biophys. Res. Commun.* **2002**, *291*, 535–541.
17. Kickhoefer, V. A.; Garcia, Y.; Mikyas, Y.; Johansson, E.; Zhou, J. C.; Raval-Fernandes, S.; Minoofar, P.; Zink, J. I.; Dunn, B.; Stewart, P. L.; Rome, L. H. Engineering of Vault Nanocapsules with Enzymatic and Fluorescent Properties. *Proc. Natl. Acad. Sci. U.S.A.* **2005**, *102*, 4348–4352.
18. Kickhoefer, V. A.; Han, M.; Raval-Fernandes, S.; Poderycki, M. J.; Moniz, R. J.; Vaccari, D.; Silvestry, M.; Stewart, P. L.; Kelly, K. A.; Rome, L. H. Targeting Vault Nanoparticles to Specific Cell Surface Receptors. *ACS Nano* **2009**, *3*, 27–36.
19. Beari, F.; Brand, M.; Jenkner, P.; Lehnert, R.; Metternich, H. J.; Monkiewicz, J.; Siesler, H. W. Organofunctional Alkoxysilanes in Dilute Aqueous Solution: New Accounts on the Dynamic Structural Mutability. *J. Organomet. Chem.* **2001**, *625*, 208–216.
20. Kong, J.; Yu, S. Fourier Transform Infrared Spectroscopic Analysis of Protein Secondary Structures. *Acta Biochim. Biophys. Sin.* **2007**, *39*, 549–559.
21. Herlem, G.; Segut, O.; Antoniou, A.; Achilleos, C.; Dupont, D.; Blondeau-Patissier, V.; Gharbi, T. Electrodeposition and Characterization of Silane Thin Films from 3-(Aminopropyl)triethoxysilane. *Surf. Coat. Technol.* **2008**, *202*, 1437–1442.
22. Wong, C.; West, P. E.; Olson, K. S.; Mecartney, M. L.; Starostina, N. Tip Dilation and AFM Capabilities in the Characterization of Nanoparticles. *J. Miner. Met. Mater. Soc. (JOM)* **2007**, *59*, 12–16.
23. Lyubchenko, Y.; Shlyakhtenko, L.; Harrington, R.; Oden, P.; Lindsay, S. Atomic Force Microscopy of Long DNA: Imaging in Air and Under Water. *Proc. Natl. Acad. Sci. U.S.A.* **1993**, *90*, 2137–2140.
24. Li, X. J.; Sun, J. L.; Zhou, X. F.; Li, G.; He, P. G.; Fang, Y. Z.; Li, M. Q.; Hu, J. Height Measurement of dsDNA and Antibodies Adsorbed on Solid Substrates in Air by Vibrating Mode Scanning Polarization Force Microscopy. *J. Vac. Sci. Technol. B* **2003**, *21*, 1070–1073.
25. Maeda, Y.; Matsumoto, T.; Kawai, T. Observation of Single- and Double-Stranded DNA Using Noncontact Atomic Force Microscopy. *Appl. Surf. Sci.* **1999**, *140*, 400–405.
26. Zhou, X.; Chen, Y.; Li, B.; Lu, G.; Boey, F. Y. C.; Ma, J.; Zhang, H. Controlled Growth of Peptide Nanoarrays on Si/SiO_x Substrates. *Small* **2008**, *4*, 1324–1328.
27. Li, H.; Zhang, J.; Zhou, X.; Lu, G.; Yin, Z. ; Li, G.; Wu, T.; Boey, F.; Venkatraman, S. S. ; Zhang, H. Aminosilane Micropatterns on Hydroxyl-Terminated Substrates: Fabrication and Applications. *Langmuir*, DOI: 10.1021/la9039144.